Theoretical Modeling of $B_{12}N_{12}$ Nanocage for the Effective Removal of Paracetamol from Drinking Water

Kainat [1], Sana Gul [1], Qaisar Ali [1,*], Momin Khan [2,*], Munir Ur Rehman [2], Mohammad Ibrahim [1], Abdullah F. AlAsmari [3], Fawaz Alasmari [3] and Metab Alharbi [3]

[1] Department of Chemistry, Abdul Wali Khan University Mardan, Mardan 23200, Pakistan; kainat.chem@awkum.edu.pk (K.); sana.gul@awkum.edu.pk (S.G.); dribrahim@awkum.edu.pk (M.I.)

[2] Heilongjiang Provincial Key Laboratory of CO2 Resource Utilization and Energy Catalytic Materials, School of Material Science and Chemical Engineering, Harbin University of Science and Technology, No. 4 Linyuan Road, Harbin 150040, China; munirurrehmanafridi@gmail.com

[3] Department of Pharmacology and Toxicology, College of Pharmacy, King Saud University, Riyadh 11451, Saudi Arabia; afalasmari@ksu.edu.sa (A.F.A.); ffalasmari@ksu.edu.sa (F.A.); mesalharbi@ksu.edu.sa (M.A.)

* Correspondence: qaisarjann@gmail.com (Q.A.); mominkhan@awkum.edu.pk (M.K.)

Abstract: In our current investigation, we employed a $B_{12}N_{12}$ nanocage to extract paracetamol from water utilizing a DFT approach. We explored three distinct positions of paracetamol concerning its interaction with the $B_{12}N_{12}$ nanocage, designated as complex-1 (BNP-1), complex-2 (BNP-2), and complex-3 (BNP-3), under both aqueous and gaseous conditions. The optimized bond distances exhibited strong interactions between the nanocage and the paracetamol drug in BNP-1 and BNP-3. Notably, BNP-1 and BNP-3 displayed substantial chemisorption energies, measuring at -27.94 and -15.31 kcal/mol in the gas phase and -30.69 and -15.60 kcal/mol in the aqueous medium, respectively. In contrast, BNP-2 displayed a physiosorbed nature, indicating weaker interactions with values of -6.97 kcal/mol in the gas phase and -4.98 kcal/mol in the aqueous medium. Our analysis of charge transfer revealed significant charge transfer between the $B_{12}N_{12}$ nanocage and paracetamol. Additionally, a Quantum Theory of Atoms in Molecules (QTAIM) analysis confirmed that the O–B bond within BNP-1 and BNP-3 exhibited a strong covalent and partial bond, encompassing both covalent and electrostatic interactions. In contrast, the H–N bond within BNP-2 displayed a weaker hydrogen bond. Further investigation through Noncovalent Interaction (NCI) and Reduced Density Gradient (RDG) analyses reinforced the presence of strong interactions in BNP-1 and BNP-3, while indicating weaker interactions in BNP-2. The decrease in the electronic band gap (E_g) demonstrated the potential of $B_{12}N_{12}$ as a promising adsorbent for paracetamol. Examining thermodynamics, the negative values of ΔH (enthalpy change) and ΔG (Gibbs free energy change) pointed out the exothermic and spontaneous nature of the adsorption process. Overall, our study underscores the potential of $B_{12}N_{12}$ as an effective adsorbent for eliminating paracetamol from wastewater.

Keywords: DFT; boron nitride nanocage; paracetamol; adsorption

1. Introduction

Water resources are of prime importance in developing countries because they are used domestically and in agriculture and industry. Water is polluted by manmade and natural sources, which has serious impacts on human health [1]. Natural sources contribute to water pollution by adding contaminants that are present in water supplies. On the other hand, manmade sources such as agricultural practices, unsuitable disposal of wastewater, industrial activities, and sewage systems also contribute to water pollution. Both manmade and natural sources contaminate water, threatening water purity and safety. Water pollutants includes heavy metals, chemical pollutants, pesticides, and medicines, which are continuously being studied, and the introduction of new chemicals, pesticides, and

medicines poses additional difficulties [2,3]. Numerous studies have been carried out to probe the quality of groundwater and to investigate the related health issues as drinking polluted water has serious effects on human health [4–8].

Pharmaceutically active compounds are emerging pollutants that can be detected in surface water, drinking water, industrial and domestic water, and groundwater [9]. Pharmaceutically active compounds include antibiotics (ciprofloxacin, levofloxacin, nalidixic acid), nonsteroidal anti-inflammatory drugs (NSAIDs) (diclofenac, ibuprofen, naproxen), hormones, and antidepressants (meprobamate, diazepam). A very large quantity of pharmaceuticals is used around the globe to cure animal and human diseases in feedstock facilities, households, hospitals, and agriculture. However, they are not completely absorbed in the body, and the unabsorbed and unmetabolized pharmaceuticals are excreted, which finally contaminates the ground- and surface water. Similarly, the inappropriate disposal of unwanted drugs and expired ones is another source of water pollution [10]. Such contaminated wastewater is subjected to treatment in wastewater treatment plants (WWTPs), which are unable to eliminate the pharmaceuticals completely to make it suitable for drinking. In Madrid (Spain), a considerable quantity of NSAIDs was found in drinking water after treatment in WWTPs that treated wastewater in an area with pharmaceutical industries, university campuses, and hospitals [11]. Paracetamol, also known as acetaminophen, is one of the most extensively used analgesic and antipyretic drugs among over-the-counter (OTC) and most frequently prescribed drugs [12,13]. The global market for acetaminophen is expected to be value at USD 121.7 million by 2018 [14]. Paracetamol is one of the most rapidly growing emerging contaminants on the globe, and its existence has been reported earlier to be up to 200 µg/L and 28.70 µg/L in wastewater effluents and surface water, respectively [15], despite its high removal capacity of about 90% in WWTPs [16–18]. Researchers reported a strong tendency of paracetamols and other NSAIDs toward accumulation, sorption, and persistence in soil sediments and plants [19,20] and reported a number of toxicities of paracetamols in plants, soil, and aquiculture [21]. Different methodologies have been applied to eliminate pharmaceuticals from drinking water including membrane filtration, membranes with sorption capabilities, advanced oxidation, and adsorption [22,23]. Adsorption is the most commonly used method due to its ease of operation, low energy usage, low cost, and high efficiency [24–27]. Different adsorbents of a 2D and 3D nature have been applied for the removal of pharmaceuticals from wastewater [28]. Adsorbents such as single- and multiwall carbon-based nanotubes, graphene, activated carbon, chitosan-grafted graphene oxide composites, TiO_2/GO composites, biochar, magnetic mesoporous carbon, and graphene oxide have been utilized for the adsorption of pharmaceuticals with desirable results [29–32]. However, these nanomaterials possess numerous issues, i.e., low hydrophobicity of carbon nanotubes and long-term sustainability, which make the nanomaterials difficult to separate from water and toxic to the ecosystem [33–37]. In recent research, aluminum nitride and boron nitride nanotubes were explored as the most appropriate candidates for the elimination of a large number of pollutants from wastewater due to their thermal and structural stability, high hydrophobicity, wide band gap, and resistance to oxidation [38–40]. Likewise, inorganic nanocages such as $Al_{12}N_{12}$ and $B_{12}N_{12}$ have been employed for the adsorption of pollutants due to their distinctive surface and their physical and chemical properties [41–44]. They were used experimentally for the abatement of aspirin [45] and for the removal of toxic gases like NH_3, ClCN, and HCN [46,47]. Additionally, $Al_{12}P_{12}$ nanocages were used for the effective sensing of CH_3Cl and CH_3F [48]. The $B_{12}N_{12}$ nanocage [49] was synthesized by employing the arc-melting method from YB_6 powder, and four- and six-membered rings were found in the nanocage. The $B_{12}N_{12}$ nanocage possesses substantial properties such as oxidation resistance, structural and thermal stability, and high surface area and can be used effectively for the abatement of paracetamol from wastewater.

In the present work, we examined the interaction of paracetamol with a $B_{12}N_{12}$ nanocage using density functional theory (DFT) calculations. DFT analyses such as bond elongation, bond length, atoms in molecule, thermodynamics, electron density difference,

and charge transfer analyses were used to study the interaction of paracetamol with the $B_{12}N_{12}$ nanocage, and we found promising results. This study will open new routes of research for the removal of emerging pollutants using $B_{12}N_{12}$ nanocages.

2. Computational Details

The structures of the adsorbent and the adsorbate were built using the free advanced chemical editor software Avogadro 1.2.0 and optimized initially using the auto-optimization tool [50]. An input file for each monomer was prepared using RUNTYP = OPTIMIZE and the tight convergence option for the GAMESS US program [51]. All the structures were subsequently optimized employing B3LYP theory with a 631-G(d,p) basis set through the GAMESS US program. To form complexes of the adsorbent with the drug, the optimized geometries of the monomers were used in the Avogadro software, and the complexes were optimized using the same protocols through the GAMESS US program. To modify the adsorption energies of all complexes, the DFT-D3 (dispersion correction) scheme of Grimme was used [52]. Then, for all complexes, the adsorption energies were obtained through the following equation:

$$E_{ads} = E_{complex} - \left(E_{nanocage} + E_{paracetamol} \right), \tag{1}$$

where $E_{nanocage}$ and $E_{paracetamol}$ stands for the total electronic energies of the nanocage and the paracetamol, respectively, and $E_{complex}$ represents the total electronic energy of the optimized complex systems.

Noncovalent interaction (NCI) analysis [53] was carried out using the Multiwfn program [54] and visualized using the VMD 1.9.4a51 software [55] to detect the electrostatic interactions and H-bonds between the adsorbent and adsorbate. Reduced density gradient (RDG) analysis [53] using the Multiwfn program [54] was performed to justify the existence of strong or weak interactions between the adsorbents and adsorbates. Natural bonding orbital analysis with the help of NBO code in Gaussian 16 [56] was used for the analysis of charges, which were used to investigate the charge transfer. In order to assess the influence of the medium on the adsorption of the drug onto the $B_{12}N_{12}$ nanocage, we conducted investigations in an aqueous medium using a polarizable continuum model (PCM) and obtained the adsorption energies [57]. All the DFT simulations were performed using the B3LYP/631-G(d,p) basis set [58]. Quantum theory of atoms in molecules (QTAIM) analysis was employed to study the strength and behavior of the interaction. Furthermore, various topological parameters were computed at the bond-critical points (BCPs) specifically kinetic electron density (G_b), Laplacian ($\nabla^2 \rho_b$), electron densities (ρ_b), total electron energy densities (H_b), and potential electron energy density (V_b) using the Multiwfn program [54] from the wfn file obtained in Gaussian 16 programs [56]. The sensing ability of the adsorbent for the adsorbate was evaluated using frontier molecular orbital (FMO) analysis. The following equation was used for the calculation of the bandgap (E_g) values for all the complexes:

$$E_g = E_{LUMO} - E_{HOMO}, \tag{2}$$

where E_g refers to the bandgap or energy gap and $LUMO$ and $HOMO$ denote the lowest unoccupied molecular orbitals and the highest occupied molecular orbitals, respectively.

The Multiwfn 3.6(dev) software and Gaussian 16 [54,56] were used to visualize the overlap of orbitals, which were simulated using energy density difference (EDD) analysis. To study the effect of an aqueous medium on the adsorption process, calculations were carried out by using a polarizable continuum model (PCM) in the GAMESS UK code [51]. Thermodynamics simulations with the RUNTYP = HESSIAN option in the input file of the GAMESS code were employed to study the feasibility and nature (spontaneous/nonspontaneous) of the adsorption process. The enthalpy change (ΔH) and

the Gibbs free energy (ΔG) were determined by employing the following equations to determine the thermodynamics of the adsorption process:

$$\Delta H_{ads} = H_{Complex} - H_{(nanocage+paracetamol)}, \tag{3}$$

$$\Delta G_{ads} = \Delta H_{ads} - T\Delta S_{ads}, \tag{4}$$

$$\Delta G_{ads} = \Delta H_{ads} - T\left(S_{(complex)} - \left(S_{nanocage} + S_{paracetamol}\right)\right), \tag{5}$$

where G represents the total electronic and thermal Gibbs free energy, H symbolizes the total electronic and thermal enthalpy, and S refers to the entropy at a temperature of 298.15 K and a pressure of 1 atm.

The time required for the adsorbents in all complexes to regenerate or recover was assessed using the following equation:

$$\tau = v_0^{-1} exp(-E_{ads}/kT), \tag{6}$$

where v_0^{-1} denotes the attempt frequency, E_{ads} refers to the adsorption energy, T stands for temperature, and k represents Boltzmann's constant.

2.1. Optimization of Geometry of $B_{12}N_{12}$ Nanocage and Paracetamol

Figures 1 and 2 illustrate the optimized geometries of paracetamol and $B_{12}N_{12}$ along with their resultant molecular electrostatic potential (MEP) map. It has been reported in the literature that the bond length between B and N in the tetragon is 1.49 and the bond length in the hexagon ring is 1.43 Å, respectively [59].
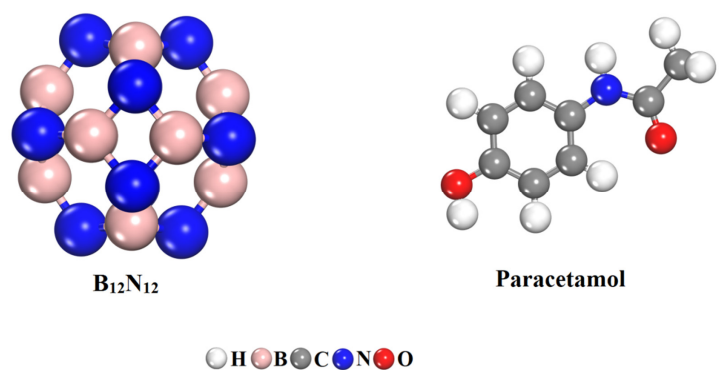
Figure 1. Optimized geometry of $B_{12}N_{12}$ nanocage and paracetamol.
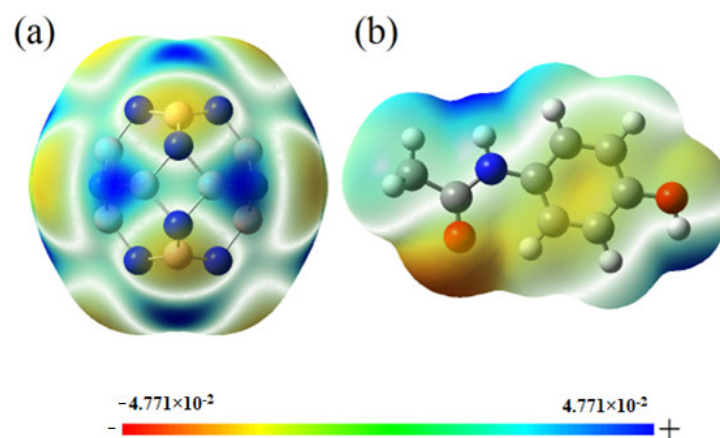
Figure 2. MEP map of $B_{12}N_{12}$ nanocage (**a**) and paracetamol (**b**).

2.2. Optimization of $B_{12}N_{12}$ Complexes and Estimation of Binding Energies

Based on the MEP map displayed in Figure 3, it is clear that the C=O and O–H groups in the paracetamol drug and the B and N atoms within the $B_{12}N_{12}$ cage are identified as a hot site for potential interactions. In the MEP map, regions colored red indicate electrophilic centers while those in blue indicate the nucleophilic centers. Therefore, we targeted these sites for interactions in our present study.
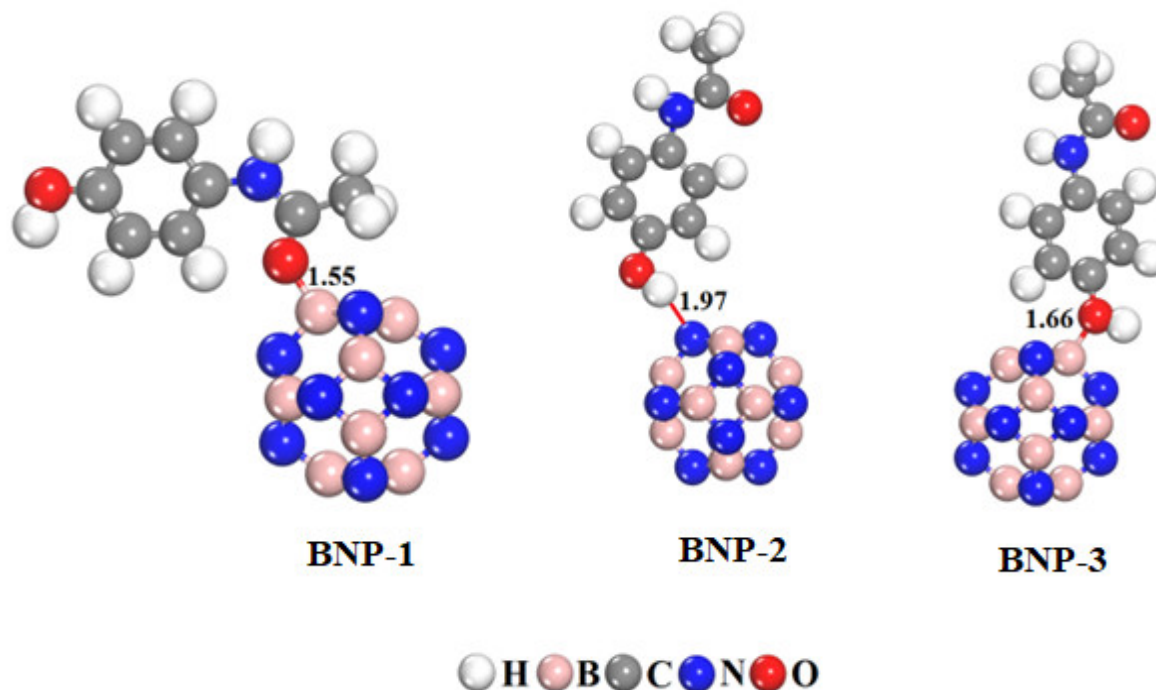
Figure 3. Optimized complexes of $B_{12}N_{12}$ nanocage with paracetamol.

As a result, we investigated three distinct interaction modes between paracetamol and $B_{12}N_{12}$, labeled as complex-1 (BNP-1), complex-2 (BNP-2), and complex-3 (BNP-3). The optimized configurations of all the above-mentioned complexes are illustrated in Figure 3. In BNP-1, the boron atom of the nanocage forms a bond with the oxygen atom (O) of the C=O group of the adsorbate, resulting in a computed O–B bond length of 1.55 Å. In BNP-2, the calculated bond length between the H atom of O–H and the nanocage was 1.97 Å, while in BNP-3, the bond length between the O atom of O–H and the boron atom of the nanocage was observed to be 1.66 Å. The adsorption energies of BNP-1 and BNP-3 indicate that they interact via chemisorption, with an E_{ads} of −27.94 kcal/mol, whereas the adsorption energy of BNP-2 shows that it interacts via physisorption, having E_{ads} values of 15.3125 kcal/mol as mentioned in Table 1.

Table 1. Adsorption energies (E_{ads}), frontier molecular orbital (FMO), and charge transfer (Q) analyses of the optimized complexes of $B_{12}N_{12}$ with paracetamol.

System	E_{ads}	E_{LUMO}	E_{HOMO}	E_g	Q
$B_{12}N_{12}$	-	−0.84	−7.70 eV	6.86 eV	-
Paracetamol	-	−0.08	−5.48	5.40	-
BNP-1	−27.94	−1.72	−6.52	4.80	−0.018
BNP-2	−6.97	−1.11	−5.26	4.15	0.017
BNP-3	−15.31	−0.95	−6.53	5.58	−0.041

Frontier molecular orbital study of the complexes of the $B_{12}N_{12}$ nanocage and paracetamol. The adsorption energies are in Kcal/mol; the *HOMO*, *LUMO*, and E_g are in eV; and the ΔQ_{CT} is in e.

The results concerning the values of the adsorption energies indicate that paracetamol forms a strong interaction through the O of its C=O bond. This strong interaction is due to a covalent bond, which is supported by small bond length values in BNP-1. On the other hand, a weak hydrogen bond exists in BNP-2 as indicated by small bond length values and small E_{ads} values. In contrast, BNP-3 exhibits a strong interaction of a partial nature, having both electrostatic and covalent interactions, leading to chemisorption with small bond length values. Furthermore, electrostatic interactions at other positions in BNP-1 and BNP-3 contribute to the overall E_{ads} values, highlighting a strong interaction in these complexes.

2.3. Reduced Density Gradient (RDG) Analysis and Noncovalent Interaction (NCI)

Figure 4 represents the two-dimensional figures of the reduced density gradient (RDG) and three-dimensional figures of the noncovalent interaction (NCI) for the complexes of paracetamol and $B_{12}N_{12}$. The 2D and 3D plots use color-coded spots to indicate the weak and strong noncovalent interactions and steric repulsion in the observed complexes. The RDG plot displays spikes with values of (sign λ2) ρ < 0, indicating strong interactions. Specifically, in the RDG figure, the green-encircled spikes in BNP-1 and BNP-3 indicate the occurrence of an electrostatic interaction between the hydrogen atom of the paracetamol and the nitrogen atom of the $B_{12}N_{12}$ nanocage. On the other hand, the black-encircled spikes in BNP-1 and BNP-3 suggest a strong covalent and partial interaction, while the red-encircled spikes in all three complexes indicate repulsion between the atoms.
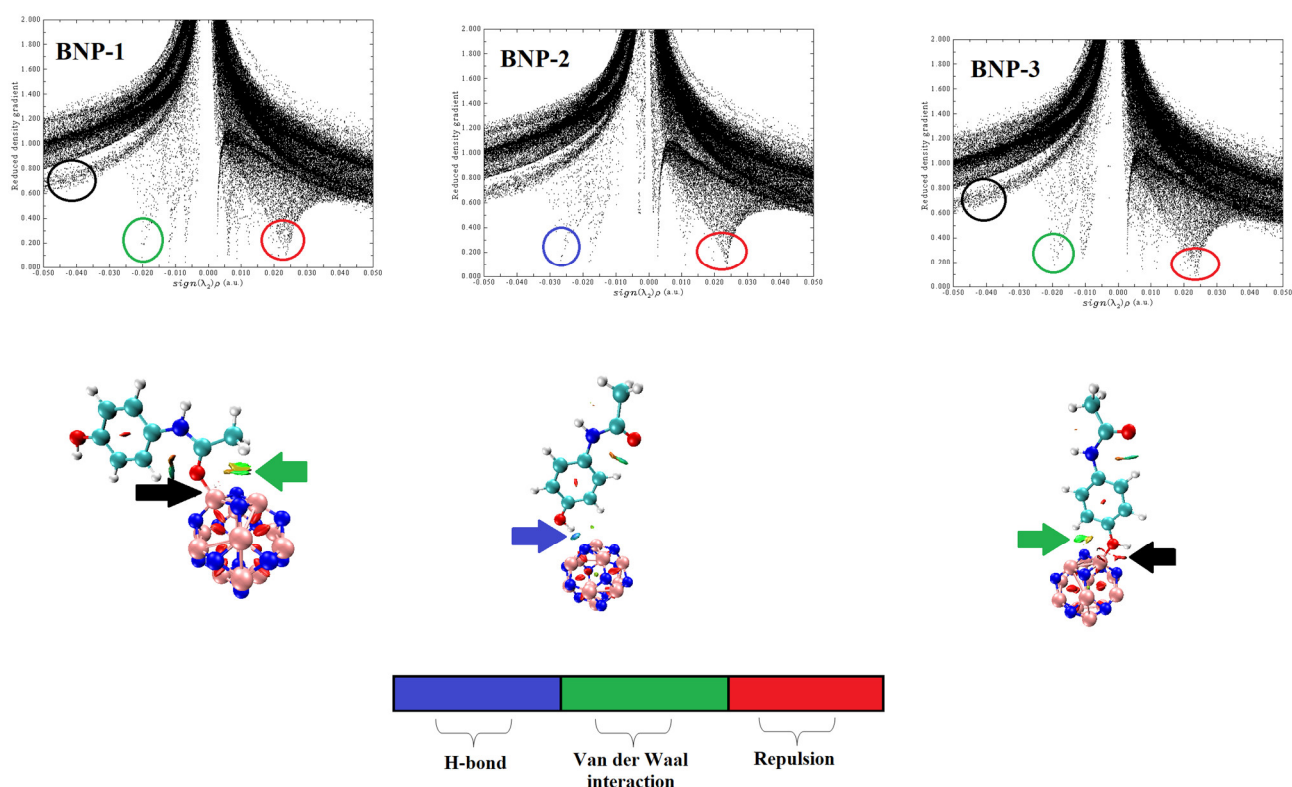
Figure 4. RDG and NCI analysis of complexes of $B_{12}N_{12}$ nanocage with paracetamol.

Regarding the NCI plots, the blue-encircled spike in BNP-2 signifies a weak hydrogen bond, which is responsible for physisorption. The existence of a strong bond in the NCI figure is represented by two black arrows in BNP-1 and BNP-2 showing the bond between the interacting atoms. These strong interactions were also evident in the 3D plots. The two green arrows in BNP-1 and BNP-2 point to the green-colored region between the interaction of the H atom of the paracetamol and the N atom of the $B_{12}N_{12}$ nanocage,

representing electrostatic interactions. Similarly, a weak hydrogen bond is demonstrated by the blue arrow pointing to the blue-colored region between the hydrogen atom of O–H of the paracetamol and the nitrogen atom of the $B_{12}N_{12}$ nanocage. Furthermore, the presence of the red-colored region between the atoms of the paracetamol and the nanocage in the NCI map indicates repulsion between atoms at various positions in the complexes.

Based on the RDG and NCI analyses, it can be concluded that strong interactions are present in BNP-1 and BNP-3, while BNP-2 exhibits a weak hydrogen bond.

2.4. Natural Bonding Orbital (NBO) Analysis

The sensing abilities of the $B_{12}N_{12}$ nanocage concerning the paracetamol drug were assessed using the widely recognized natural bonding orbital (NBO) method. The results obtained were then compared with the charges of atoms in the isolated nanocage and paracetamol, and these findings are tabulated as Table 1. In this context, the charge transfer refers to the charge variations between the paracetamol/$B_{12}N_{12}$ structure and the nanocage alone. The data presented in Table 1 reveal a significant charge transfer (ΔN) from the donor hydrogen and oxygen atoms of paracetamol and to the acceptor boron and nitrogen atoms of the $B_{12}N_{12}$ nanocage.

The analysis of natural bonding orbitals (NBOs) reveals that the charges on the oxygen (O) and hydrogen (H) atoms of paracetamol in BNP-1 and BNP-2 and the charge on the oxygen (O) atom in BNP-3 decrease from -0.625, 0.508, and -0.694 e to -0.607, 0.491, and -0.653, respectively. This indicates a net charge transfer of -0.018, 0.017, and -0.041 from paracetamol to the $B_{12}N_{12}$ nanocage. Notably, the charge transfer is more significant in BNP-1 and BNP-3 as compared to BNP-2, suggesting a strong interaction between paracetamol and the $B_{12}N_{12}$ nanocage. These results are consistent with the findings obtained from the E_{ads} values, the bond length analysis, and the NCI and RDG analyses.

2.5. Quantum Theory of Atoms in Molecules (QTAIM) Analysis

The strength and nature of interactions between paracetamol and the $B_{12}N_{12}$ nanocage were extensively examined using QTAIM analysis. Figure 5 [9] illustrates the QTAIM figures with bond-critical points, which provided insight to various topological parameters at this point. These parameters, including the kinetic electron density (G_b), Laplacian ($\nabla^2\rho_b$), electron densities (ρ_b), total electron energy densities (H_b), and potential electron energy density (V_b), were carefully analyzed to characterize the interactions as either covalent or weak electrostatic involving electron sharing or transfer [15]. At the bond-critical points (BCPs), a positive value of H_b indicates closed-shell interactions while a negative value suggests covalent interaction between the adsorbent and the adsorbate. If both values, i.e., H_b and $\nabla^2\rho_b$, are positive, then it indicates the occurrence of weak electrostatic interaction. Meanwhile, if both the values are negative, it indicates the presence of a covalent bond, but if the value of $\nabla^2\rho_b$ is positive and H_b is negative, it indicates the partial existence of both covalent and electrostatic interactions. Furthermore, the nature of interactions can be classified as weak electrostatic and noncovalent if the ratio $-G_b/V_b$ has values greater than unity. On the other hand, the interactions are considered strong covalent if the values are less than unity and partial if the values are less then unity but greater than 0.5.

Table 2 presents our computed results, showing the H_b values at BCPs 67, 52, and 52 in BNP-1, BNP-2, and BNP-3, respectively. These values indicate closed-shell interactions between the adsorbent and the adsorbate. Notably, the highest electron density (ρ_b) at BCP 67 in BNP-1 suggests strong interaction among all complexes. Similarly, the larger ρ_b values at BCP 52 in BNP-3 indicate a strong bond compared to BNP-2. Additionally, the negative $\nabla^2\rho_b$ and H_b values at BCP 67 in BNP-1 signify a strong covalent interaction, while at BCP 52 in BNP-3, the results indicate partial interaction involving both covalent and electrostatic forces, as reflected by the negative H_b values and positive $\nabla^2\rho_b$ values. These findings are consistent with the $-G_b/V_b$ ratio, which is less than 0.5 at BCP 67 and greater than 0.5 but less than unity at BCP 52.
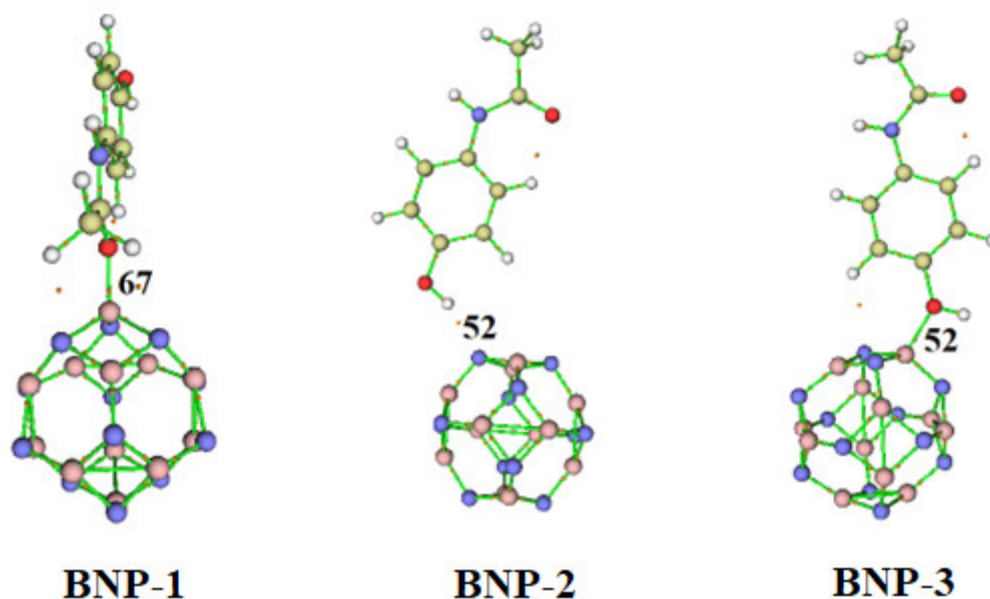
Figure 5. QTAIM analysis of complexes of $B_{12}N_{12}$ nanocage with paracetamol.

Table 2. QTAIM analysis of complexes of $B_{12}N_{12}$ nanocage with paracetamol.

System	BCP	Density of All Electrons (ρ_b)	Laplacian ($\nabla^2\rho_b$)	Kinetic Electron Density G_b	Potential Energy Density V_b	Energy Density H_b	$-G_b/V_b$
BNP-1	67	0.34	−0.96	0.32	−0.89	−0.56	0.36
BNP-2	52	0.03	0.07	0.02	−0.02	−0.0004	0.97
BNP-3	52	0.09	0.28	0.12	−0.17	−0.05	0.70

Bond-critical points (BCPs), electron density (ρ au), Laplacian ($\nabla^2\rho b$ au), kinetic electron density (G_b au), potential energy density (V_b au), energy density (H_b au), and ratio of kinetic electron density and potential energy density ($-G_b/V_b$ au).

The results obtained from the QTAIM analysis align with the outcomes of the DFT (Density Functional Theory) analysis, providing further evidence of the efficiency of the $B_{12}N_{12}$ nanocage in the removal of paracetamol from wastewater.

2.6. Frontier Molecular Orbital (FMO) Analysis

The confirmation of the binding of paracetamol onto the $B_{12}N_{12}$ nanocage was further studied by analyzing the frontier molecular orbitals (HOMO–LUMO) of the nanocage, paracetamol, and complexes. The corresponding figures and results can be found in Figure 6 and Table 1, respectively. According to Figure 6, the $B_{12}N_{12}$ nanocage demonstrates distinct HOMO and LUMO distribution, with the HOMO predominantly spread over the nitrogen atom while the LUMO is localized on the boron atom. The binding of paracetamol onto the $B_{12}N_{12}$ nanocage induces remarkable changes in the HOMO–LUMO distribution. In the cases of BNP-1, BNP-2, and BNP-3, the LUMO is primarily concentrated on the cyclic ring of the paracetamol, while the HOMO involves the O–H and the cyclic ring, with a particular focus on the interacting position in BNP-1 and BNP-3. These observations indicate substantial charge transfer and a strong interaction between paracetamol and the $B_{12}N_{12}$ nanocage. On the other hand, the HOMO exhibits marginal separation from the interacting atoms of both the paracetamol and the $B_{12}N_{12}$ nanocage, leading to minimal orbital overlap and negligible charge transfer. These observations suggest very weak interactions in these cases.
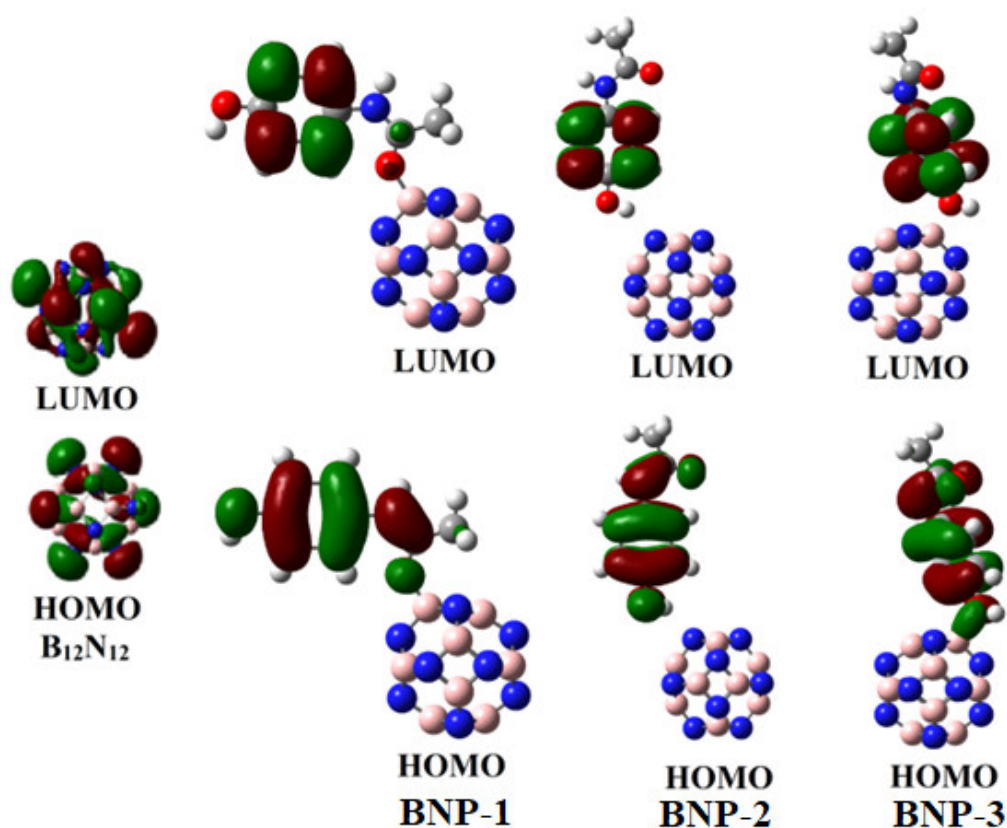
Figure 6. HOMO–LUMO map of complexes of $B_{12}N_{12}$ nanocage with paracetamol.

The $B_{12}N_{12}$ nanocage exhibits HOMO and LUMO energy values of −7.70 eV and −0.84 eV, respectively, resulting in a HOMO–LUMO gap of 6.68 eV. Upon complexation with BNP-1, the HOMO energy value decreased from 7.70 eV to −6.52 eV, while the LUMO energy value increased from 0.84 eV to 1.72 eV, resulting in a reduced energy gap of 4.80 eV. This change in energy gap is expected to increase the sensitivity of the $B_{12}N_{12}$ nanocage toward the drug, i.e., paracetamol. Similarly, for BNP-2 and BNP-3, the HOMO energies decreased to −5.26 eV and −6.53 eV, respectively, while the LUMO energies increased to −1.11 eV and −0.95 eV, leading to decreased energy gaps of 4.15 eV and 5.58 eV, respectively. These significant variations in the energy gaps indicate that the $B_{12}N_{12}$ nanocage effectively sensed the paracetamol molecule. The reduction in the energy gap in the complexes strongly suggests favorable attractions and the possible overlap of atomic orbitals, indicating the enhanced electrical conductivity and sensitivity of the $B_{12}N_{12}$ nanocage toward the paracetamol drug.

2.7. Electron Density Difference (EDD) Analysis

The electron density difference (EDD) analysis was performed to investigate the intermolecular interactions between the paracetamol and the $B_{12}N_{12}$ nanocage. Figure 7 illustrates the plot of the EDD for all three complexes. The EDD was performed by calculating the difference in electron density between the complexes and sum of the isolated species, namely, paracetamol and the $B_{12}N_{12}$ nanocage. The ED of the individual species is determined by using the coordinates from the relaxed geometries of the complexes. The EDD plots of the complexes reveal blue and green regions, which signify the orbital contact between the paracetamol and the $B_{12}N_{12}$ nanocage. Furthermore, BNP-1 and BNP-3 show a huge green loop between the interaction sites of paracetamol and the $B_{12}N_{12}$ nanocage, providing strong evidence of significant interactions and substantial charge transfer from paracetamol to the $B_{12}N_{12}$ nanocage. In BNP-2, the size of the blue and green loops is very

small, indicating minimal overlap and weak interactions. These findings from the EDD analysis are consistent with the charge transfer analysis.
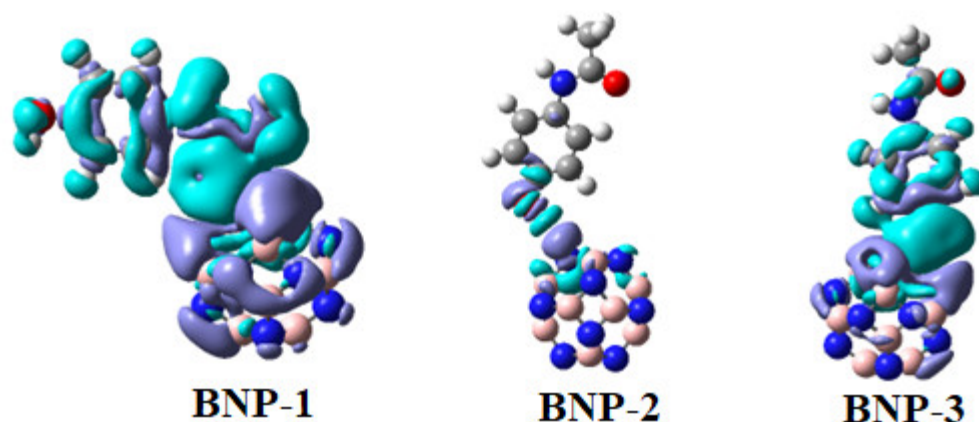
Figure 7. EDD map of complexes of $B_{12}N_{12}$ nanocage with paracetamol.

2.8. Effect of Solvent on the Adsorption and Dipole Moment Analysis

The results of the PCM analysis show that the water has a minimal effect on the interaction between the paracetamol and the $B_{12}N_{12}$ nanocage. The calculated E_{ads} values for BNP-1, BNP-2, and BNP-3 in the aqueous medium were -30.69, -4.98, and -15.60 kcal/mol, respectively. These values suggest that water has a minimal effect on the adsorption process, and it further confirms the stable interaction between paracetamol and the $B_{12}N_{12}$ nanocage in the aqueous medium. Table 3 lists the variations in the dipole moment (DM) between the $B_{12}N_{12}$ nanocage and the complexes. It is worth noting that the dipole moment of the free $B_{12}N_{12}$ nanocage is zero due to its symmetrical structure. However, when paracetamol is involved, the dipole moment increases noticeably, indicating a noteworthy charge separation between the paracetamol and the $B_{12}N_{12}$ nanocage. The results strongly suggest that the aqueous phase is more favorable than the gas phase. Among the complexes, BNP-1 and BNP-3 exhibit the highest increase in dipole moment, which is consistent with their large E_{ads} values and short bond lengths. On the other hand, BNP-2 shows a slight increase in the dipole moment, revealing a physisorption nature and supporting the smallest E_{ads} values. The study of the dipole moment provides evidence of charge transfer between paracetamol and the $B_{12}N_{12}$ nanocage.

Table 3. Adsorption energy (E_{ads}) in gas and aqueous medium, dipole moment, and thermodynamics analysis of complexes of $B_{12}N_{12}$ with paracetamol.

System	E_{ads} (Gas Medium)	E_{ads} (Water Medium)	DM	ΔH	ΔG
$B_{12}N_{12}$	-	-	0.000010	-	-
BNP-1	-27.94	-30.69	11.14	-21.52	-19.13
BNP-2	-6.97	-4.98	1.62	-2.41	-1.03
BNP-3	-15.31	-15.60	7.72	-10.31	-7.59

The adsorption energies (gas phase and aqueous medium), enthalpy change (ΔH), and free energy change (ΔG) are in Kcal/mol; the dipole moment is in Debye.

3. Thermodynamics Analysis

The nature and feasibility of the binding of paracetamol on the nanocage is better understood through thermodynamics analysis, which involves studying changes in the enthalpy, entropy, and free energy. These parameters play a crucial role in practical applications of the binding of paracetamol on the nanocage. In Table 3, we present the results of our simulations for ΔH and ΔG, all of which showed negative values for all the three complexes (BNP-1, BNP-2, and BNP-3). This indicates that the adsorption process is exothermic

and spontaneous. The thermodynamics parameters align well with the energetic analysis, affirming the exothermic and feasible nature of the process.

4. Recovery Time Calculation

In this research, we extensively examined the adsorbent's efficiency by determining the recovery times for the three complexes at two different temperatures 298.15 and 350 K. Our findings revealed that BNP-2 exhibited the shortest recovery time, while BNP-1 displayed the longest recovery time both at 298.15 and 350 K as shown in Figure 8. The regeneration study results highlight the $B_{12}N_{12}$ adsorbent's fast renewal rate at room temperature, making it a highly suitable candidate for the efficient removal of paracetamol from wastewater due to its exceptional and stable characteristics.
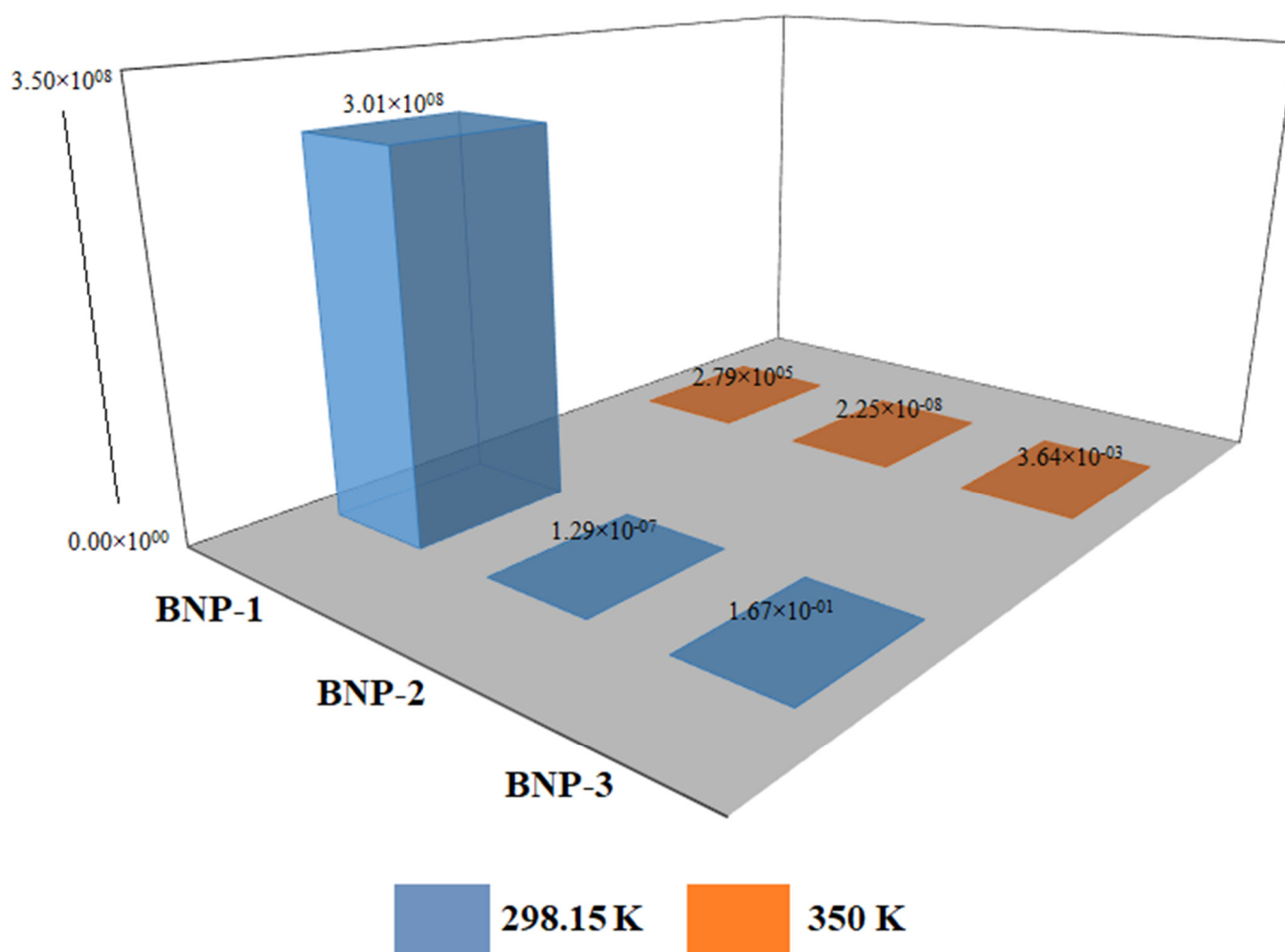
Figure 8. Recovery time graph of complexes of $B_{12}N_{12}$ nanocage with paracetamol.

5. Conclusions

In the current study, density functional theory simulations were utilized to examine the interaction between paracetamol and the $B_{12}N_{12}$ nanocage, evaluating its sensing capabilities for the abatement of the paracetamol drug from wastewater. The geometry analysis and bond length analysis indicated that BNP-1 and BNP-3 form strong bonds with the $B_{12}N_{12}$ nanocage, while BNP-2 shows a weak interaction. The charge transfer analysis demonstrated noteworthy charge transfer, supported by frontier molecular orbital (FMO) and electron density difference (EDD) analysis, which depicted orbital overlap. The quantum theory of atoms in molecules (QTAIM) analysis revealed strong bonds in

BNP-1 and BNP-3, while there was a weak hydrogen bond in BNP-2. Negative values of ΔH and ΔG indicated an exothermic, feasible, and spontaneous adsorption process at room temperature. These results were further supported by reduced density gradient and noncovalent interaction analyses. The increase in the dipole moment of the complexes further confirmed the interaction between the paracetamol and the $B_{12}N_{12}$ nanocage. The regeneration study demonstrated the absorbent's ease of regeneration and reusability. Overall, this study demonstrated a strong binding interaction between $B_{12}N_{12}$ and paracetamol, which represents an initial stride toward exploring $B_{12}N_{12}$'s potential as a candidate for pharmaceutical removal from wastewater.

Supplementary Materials: The following supporting information can be downloaded at https://www.mdpi.com/article/10.3390/computation11090183/s1: Table S1. Grimme's dispersion energy of the complexes.

Author Contributions: Conceptualization, M.K.; Data curation, Q.A. and F.A.; Formal analysis, M.U.R.; Investigation, M.U.R. and M.A.; Methodology, K. and S.G.; Resources, A.F.A. and M.A.; Software, Q.A. and F.A.; Validation, M.I; Writing—original draft, M.K.; Writing—review and editing, M.I. and A.F.A. All authors have read and agreed to the published version of the manuscript.

Funding: This Research was funded by researcher's supporting project number RSP2023R235, King Saud University, Riyadh, Saudi Arabia.

Data Availability Statement: All data generated or analyzed during this study are included in this published article and Supplementary Materials.

Acknowledgments: The authors are thankful to researcher's supporting project number RSP2023R235, King Saud University, Riyadh, Saudi Arabia.

Conflicts of Interest: The authors declare no conflict of interest.

References

1. Babuji, P.; Thirumalaisamy, S.; Duraisamy, K.; Periyasamy, G. Human Health Risks due to Exposure to Water Pollution: A Review. *Water* **2023**, *15*, 2532. [CrossRef]
2. Guo, W.; Li, P.; Du, Q.; Zhou, Y.; Xu, D.; Zhang, Z. Hydrogeochemical processes regulating the groundwater geochemistry and human health risk of groundwater in the rural areas of the Wei River Basin, China. *Expo. Health* **2023**, 1–16. [CrossRef]
3. Liu, L.; Wu, J.; He, S.; Wang, L. Occurrence and distribution of groundwater fluoride and manganese in the Weining Plain (China) and their probabilistic health risk quantification. *Expo. Health* **2022**, *14*, 263–279. [CrossRef]
4. Alam, S.M.K.; Li, P.; Fida, M. Groundwater nitrate pollution due to excessive use of N-fertilizers in Rural Areas of Bangladesh: Pollution status, health risk, source contribution, and future impacts. *Expo. Health* **2023**, 1–24. [CrossRef]
5. Guo, Y.; Li, P.; He, X.; Wang, L. Groundwater quality in and around a landfill in northwest China: Characteristic pollutant identification, health risk assessment, and controlling factor analysis. *Expo. Health* **2022**, *14*, 885–901. [CrossRef]
6. Li, P.; He, X.; Li, Y.; Xiang, G. Occurrence and health implication of fluoride in groundwater of loess aquifer in the Chinese loess plateau: A case study of Tongchuan, Northwest China. *Expo. Health* **2019**, *11*, 95–107. [CrossRef]
7. Li, P.; He, X.; Guo, W. Spatial groundwater quality and potential health risks due to nitrate ingestion through drinking water: A case study in Yan'an City on the Loess Plateau of northwest China. *Hum. Ecol. Risk Assess. Int. J.* **2019**, *25*, 11–31. [CrossRef]
8. Zhang, Y.; Wu, J.; Xu, B. Human health risk assessment of groundwater nitrogen pollution in Jinghui canal irrigation area of the loess region, northwest China. *Environ. Earth Sci.* **2018**, *77*, 273. [CrossRef]
9. Patel, M.; Kumar, R.; Kishor, K.; Mlsna, T.; Pittman, C.U., Jr.; Mohan, D. Pharmaceuticals of emerging concern in aquatic systems: Chemistry, occurrence, effects, and removal methods. *Chem. Rev.* **2019**, *119*, 3510–3673. [CrossRef]
10. Glassmeyer, S.T.; Hinchey, E.K.; Boehme, S.E.; Daughton, C.G.; Ruhoy, I.S.; Conerly, O.; Daniels, R.L.; Lauer, L.; McCarthy, M.; Nettesheim, T.G.; et al. Disposal practices for unwanted residential medications in the United States. *Environ. Int.* **2009**, *35*, 566–572. [CrossRef]
11. Valcárcel, Y.; Alonso, S.G.; Rodríguez-Gil, J.L.; Gil, A.; Catalá, M. Detection of pharmaceutically active compounds in the rivers and tap water of the Madrid Region (Spain) and potential ecotoxicological risk. *Chemosphere* **2011**, *84*, 1336–1348. [CrossRef] [PubMed]
12. Caragea, G.; Avram, O.; Pauna, A.; Costea, A.C.; Tudosie, M. Acetaminophen, a therapeutic or an extremely toxic remedy—A review. *J. Mind Med. Sci.* **2022**, *9*, 102–110. [CrossRef]
13. Kim, J.W.; Yoon, S.M.; Lee, S.J.; Narumiya, M.; Nakada, N.; Han, I.S.; Tanaka, H. Occurrence and fate of PPCPs wastewater treatment plants in Korea. *Int. Proc. Chem. Biol. Environ. Eng.* **2012**, *35*, 57–61.

14. Badar, Z.; Shanableh, A.; El-Keblawy, A.; Mosa, K.A.; Semerjian, L.; Al Mutery, A.; Hussain, M.I.; Bhattacharjee, S.; Tsombou, F.M.; Ayyaril, S.S.; et al. Assessment of uptake, accumulation and degradation of paracetamol in spinach (*Spinacia oleracea* L.) under controlled laboratory conditions. *Plants* **2022**, *11*, 1626. [CrossRef] [PubMed]

15. Nieto-Juárez, J.I.; Torres-Palma, R.A.; Botero-Coy, A.M.; Hernández, F. Pharmaceuticals and environmental risk assessment in municipal wastewater treatment plants and rivers from Peru. *Environ. Int.* **2021**, *155*, 106674. [CrossRef] [PubMed]

16. Ternes, T.A. Occurrence of drugs in German sewage treatment plants and rivers. *Water Res.* **1998**, *32*, 3245–3260. [CrossRef]

17. Beelen, E.S.E. *Municipal Waste Water Treatment Plant (WWTP) Effluents: A Concise Overview of the Occurrence of Organic Substances*; Association of River Waterworks-RIWA: Nieuwegein, The Netherlands, 2007; ISBN 978-90-6683-124-7.

18. Moreno-González, R.; Rodríguez-Mozaz, S.; Gros, M.; Barceló, D.; León, V.M. Seasonal distribution of pharmaceuticals in marine water and sediment from a mediterranean coastal lagoon (SE Spain). *Environ. Res.* **2015**, *138*, 326–344. [CrossRef]

19. Kummerová, M.; Zezulka, Š.; Babula, P.; Tříska, J. Possible ecological risk of two pharmaceuticals diclofenac and paracetamol demonstrated on a model plant Lemna minor. *J. Hazard. Mater.* **2016**, *302*, 351–361. [CrossRef]

20. Zheng, Y.; Sun, Z.; Liu, Y.; Cao, T.; Zhang, H.; Hao, M.; Chen, R.; Dzakpasu, M.; Wang, X.C. Phytoremediation mechanisms and plant eco-physiological response to microorganic contaminants in integrated vertical-flow constructed wetlands. *J. Hazard. Mater.* **2022**, *424*, 127611. [CrossRef]

21. Madikizela, L.M.; Ncube, S.; Chimuka, L. Uptake of pharmaceuticals by plants grown under hydroponic conditions and natural occurring plant species: A review. *Sci. Total Environ.* **2018**, *636*, 477–486. [CrossRef]

22. Gadipelly, C.; Pérez-González, A.; Yadav, G.D.; Ortiz, I.; Ibáñez, R.; Rathod, V.K.; Marathe, K.V. Pharmaceutical industry wastewater: Review of the technologies for water treatment and reuse. *Ind. Eng. Chem. Res.* **2014**, *53*, 11571–11592. [CrossRef]

23. Polak, D.; Zielińska, I.; Szwast, M.; Kogut, I.; Małolepszy, A. Modification of ceramic membranes with carbon compounds for pharmaceutical substances removal from water in a filtration—Adsorption system. *Membranes* **2021**, *11*, 481. [CrossRef] [PubMed]

24. De Andrade, J.R.; Oliveira, M.F.; da Silva, M.G.C.; Vieira, M.G.A. Adsorption of pharmaceuticals from water and wastewater using nonconventional low-cost materials: A review. *Ind. Eng. Chem. Res.* **2018**, *57*, 3103–3127. [CrossRef]

25. Dutta, S.; Gupta, B.; Srivastava, S.K.; Gupta, A.K. Recent advances on the removal of dyes from wastewater using various adsorbents: A critical review. *Mater. Adv.* **2021**, *2*, 4497–4531. [CrossRef]

26. Yu, F.; Li, Y.; Han, S.; Ma, J. Adsorptive removal of antibiotics from aqueous solution using carbon materials. *Chemosphere* **2016**, *153*, 365–385. [CrossRef]

27. Anirudhan, T.S.; Deepa, J.R.; Nair, A.S. Fabrication of chemically modified graphene oxide/nano hydroxyapatite composite for adsorption and subsequent photocatalytic degradation of aureomycine hydrochloride. *J. Ind. Eng. Chem.* **2017**, *47*, 415–430. [CrossRef]

28. El-Sayed, M.E.A. Nanoadsorbents for water and wastewater remediation. *Sci. Total Environ.* **2020**, *739*, 139903. [CrossRef]

29. Gopinath, K.P.; Vo, D.-V.N.; Prakash, D.G.; Joseph, A.A.; Viswanathan, S.; Arun, J. Environmental applications of carbon-based materials: A review. *Environ. Chem. Lett.* **2021**, *19*, 557–582. [CrossRef]

30. Zhuang, Y.; Yu, F.; Ma, J. Enhanced adsorption and removal of ciprofloxacin on regenerable long TiO_2 nanotube/graphene oxide hydrogel adsorbents. *J. Nanomater.* **2015**, *2015*, 675862. [CrossRef]

31. Li, M.; Liu, Y.; Liu, S.; Shu, D.; Zeng, G.; Hu, X.; Tan, X.; Jiang, L.; Yan, Z.; Cai, X. Cu (II)-influenced adsorption of ciprofloxacin from aqueous solutions by magnetic graphene oxide/nitrilotriacetic acid nanocomposite: Competition and enhancement mechanisms. *Chem. Eng. J.* **2017**, *319*, 219–228. [CrossRef]

32. Shi, S.; Fan, Y.; Huang, Y. Facile low temperature hydrothermal synthesis of magnetic mesoporous carbon nanocomposite for adsorption removal of ciprofloxacin antibiotics. *Ind. Eng. Chem. Res.* **2013**, *52*, 2604–2612. [CrossRef]

33. Peng, Z.; Liu, X.; Zhang, W.; Zeng, Z.; Liu, Z.; Zhang, C.; Liu, Y.; Shao, B.; Liang, Q.; Tang, W.; et al. Advances in the application, toxicity and degradation of carbon nanomaterials in environment: A review. *Environ. Int.* **2020**, *134*, 105298. [CrossRef] [PubMed]

34. Das, R.; Leo, B.F.; Murphy, F. The toxic truth about carbon nanotubes in water purification: A perspective view. *Nanoscale Res. Lett.* **2018**, *13*, 183. [CrossRef] [PubMed]

35. Sheikhi, M.; Shahab, S.; Khaleghian, M.; Kumar, R. Interaction between new anti-cancer drug syndros and CNT (6, 6-6) nanotube for medical applications: Geometry optimization, molecular structure, spectroscopic (NMR, UV/Vis, excited state), FMO, MEP and HOMO-LUMO investigation. *Appl. Surf. Sci.* **2018**, *434*, 504–513. [CrossRef]

36. Sheikhi, M.; Shahab, S.; Khaleghian, M.; Hajikolaee, F.H.; Balakhanava, I.; Alnajjar, R. Adsorption properties of the molecule resveratrol on CNT (8, 0-10) nanotube: Geometry optimization, molecular structure, spectroscopic (NMR, UV/Vis, excited state), FMO, MEP and HOMO-LUMO investigations. *J. Mol. Struct.* **2018**, *1160*, 479–487. [CrossRef]

37. Sheikhi, M.; Shahab, S.; Alnajjar, R.; Ahmadianarog, M. Adsorption properties of the new anti-cancer drug alectinib on CNT (6, 6-6) nanotube: Geometry optimization, molecular structure, spectroscopic (NMR, UV/Vis, excited state), FMO, MEP and HOMO--LUMO investigations. *J. Clust. Sci.* **2019**, *30*, 83–96. [CrossRef]

38. Kim, J.H.; Pham, T.V.; Hwang, J.H.; Kim, C.S.; Kim, M.J. Boron nitride nanotubes: Synthesis and applications. *Nano Converg.* **2018**, *5*, 17. [CrossRef]

39. Yu, S.; Wang, X.; Pang, H.; Zhang, R.; Song, W.; Fu, D.; Hayat, T.; Wang, X. Boron nitride-based materials for the removal of pollutants from aqueous solutions: A review. *Chem. Eng. J.* **2018**, *333*, 343–360. [CrossRef]

40. Yogi, R.; Jaiswal, N.K. Adsorption of CO gas molecules on zigzag BN/AlN nanoribbons for nano sensor applications. *Phys. Lett. A* **2019**, *383*, 532–538. [CrossRef]

41. Ali, Q.; Khan, A.A.; Yar, M.; Khan, M.; Ahmad, R.; Ahmad, I. Theoretical insight of ciprofloxacin removal from water using boron nitride ($B_{12}N_{12}$) nanocage. *Surf. Interfaces* **2022**, *31*, 101982. [CrossRef]

42. Tazikeh-Lemeski, E.; Soltani, A.; Baei, M.T.; Javan, M.B.; Rad, S.M. Theoretical study on pure and doped $B_{12}N_{12}$ fullerenes as thiophene sensor. *Adsorption* **2018**, *24*, 585–593. [CrossRef]

43. Rad, A.S. Study on the surface interaction of Furan with $X_{12}Y_{12}$ (X = B, Al, and Y = N, P) semiconductors: DFT calculations. *Heteroat. Chem.* **2016**, *27*, 316–322.

44. Beheshtian, J.; Kamfiroozi, M.; Bagheri, Z.; Peyghan, A.A. $B_{12}N_{12}$ nano-cage as potential sensor for NO2 detection. *Chin. J. Chem. Phys.* **2012**, *25*, 60. [CrossRef]

45. Vessally, E.; Esrafili, M.D.; Nurazar, R.; Nematollahi, P.; Bekhradnia, A. A DFT study on electronic and optical properties of aspirin-functionalized $B_{12}N_{12}$ fullerene-like nanocluster. *Struct. Chem.* **2017**, *28*, 735–748. [CrossRef]

46. Farrokhpour, H.; Jouypazadeh, H.; Sohroforouzani, S.V. Interaction of different types of nanocages ($Al_{12}N_{12}$, $Al_{12}P_{12}$, $B_{12}N_{12}$, $Be_{12}O_{12}$, $Mg_{12}O_{12}$, $Si_{12}C_{12}$ and C_{24}) with HCN and ClCN: DFT, TD-DFT, QTAIM, and NBO calculations. *Mol. Phys.* **2020**, *118*, 1626506. [CrossRef]

47. Badran, H.M.; Eid, K.M.; Ammar, H.Y. A DFT study on the effect of the external electric field on ammonia interaction with boron nitride nano-cage. *J. Phys. Chem. Solids* **2020**, *141*, 109399. [CrossRef]

48. Rad, A.S.; Zareyee, D.; Foukolaei, V.P.; Moghadas, B.K.; Peyravi, M. Study on the electronic structure of $Al_{12}N_{12}$ and $Al_{12}P_{12}$ fullerene-like nano-clusters upon adsorption of CH_3F and CH_3Cl. *Mol. Phys.* **2016**, *114*, 3143–3149.

49. Oku, T.; Nishiwaki, A.; Narita, I. Formation and atomic structure of $B_{12}N_{12}$ nanocage clusters studied by mass spectrometry and cluster calculation. *Sci. Technol. Adv. Mater.* **2004**, *5*, 635. [CrossRef]

50. Hanwell, M.D.; Curtis, D.E.; Lonie, D.C.; Vandermeersch, T.; Zurek, E.; Hutchison, G.R. Avogadro: An advanced semantic chemical editor, visualization, and analysis platform. *J. Cheminformatics* **2012**, *4*, 17. [CrossRef]

51. Wilkinson, K.A.; Sherwood, P.; Guest, M.F.; Naidoo, K.J. Acceleration of the GAMESS-UK electronic structure package on graphical processing units. *J. Comput. Chem.* **2011**, *32*, 2313–2318. [CrossRef]

52. Moellmann, J.; Grimme, S. DFT-D3 study of some molecular crystals. *J. Phys. Chem. C* **2014**, *118*, 7615–7621. [CrossRef]

53. Jumabaev, A.; Holikulov, U.; Hushvaktov, H.; Issaoui, N.; Absanov, A. Intermolecular interactions in ethanol solution of OABA: Raman, FTIR, DFT, M062X, MEP, NBO, FMO, AIM, NCI, RDG analysis. *J. Mol. Liq.* **2023**, *377*, 121552. [CrossRef]

54. Lu, T.; Chen, F. Multiwfn: A multifunctional wavefunction analyzer. *J. Comput. Chem.* **2012**, *33*, 580–592. [CrossRef] [PubMed]

55. Humphrey, W.; Dalke, A.; Schulten, K. VMD: Visual molecular dynamics. *J. Mol. Graph.* **1996**, *14*, 33–38. [CrossRef]

56. Frisch, M.J.; Trucks, G.W.; Schlegel, H.B.; Scuseria, G.E.; Robb, M.A.; Cheeseman, J.R.; Scalmani, G.; Barone, V.; Petersson, G.A.; Nakatsuji, H.; et al. *Gaussian*, 16; Gaussian Inc.: Wallingford, CT, USA, 2016.

57. Benda, R.; Vezin, T.; Lebental, B. Prediction of the interaction strength of an urea-based probe toward ions in water by means of Density Functional Theory/Polarizable Continuum Model calculations. *Int. J. Quantum Chem.* **2022**, *122*, e26901. [CrossRef]

58. Tirado-Rives, J.; Jorgensen, W.L. Performance of B3LYP density functional methods for a large set of organic molecules. *J. Chem. Theory Comput.* **2008**, *4*, 297–306. [CrossRef]

59. Noormohammadbeigi, M.; Kamalinahad, S.; Izadi, F.; Adimi, M.; Ghasemkhani, A. Theoretical investigation of thioguanine isomers anticancer drug adsorption treatment on B12N12 nanocage. *Mater. Res. Express* **2020**, *6*, 1250g2. [CrossRef]